Structure and electrochemical behavior of alkylidene-bridged metalladithiolene complexes (metals: cobalt and rhodium): bond cleavage of alkylidene moieties by electrochemical redox reactions

Chikako Takayama *, Masatsugu Kajitani, Toru Sugiyama, Akira Sugimori

Department of Chemistry, Faculty of Science and Technology, Sophia University, Kioi-cho 7-1, Chiyoda-ku, Tokyo 102-8554, Japan

Abstract

We prepared thirteen alkylidene-bridged metalladithiolene complexes $[(Cp)M(S_2C_2Y_2)(CR^1R^2)]$ (M = Co and Rh) including two novel ones. We succeeded in X-ray structure analyses of six alkylidene-bridged dithiolene complexes together with three original dithiolene complexes. The Co–S bond distance of the dithiolene ring becomes long due to the formation of alkylidene-bridged complexes. Investigation of the redox process in a series of those alkylidene-bridged metalladithiolene complexes by cyclic voltammetry reveals a large dependence for the redox potentials on the nature of M, Y and R. In the reduction, the radical anion formed in the initial process eliminates the alkylidene moiety slowly to give the radical anion of the original dithiolene complexes. One-electron oxidation gives detectable cation radicals due to some structural change, but when these cation radicals are re-reduced, they rapidly eliminate the bridging moieties to give original dithiolene complexes. We could succeed in detecting the intermediary species in the elimination process. This is one of the very rare and important successes in the trapping of the intermediate in the elimination mechanism. We conclude that both reduction and oxidation weaken the M–C and S–C bonds in the M–S–C triangle ring to regenerate the original metalladithiolene complexes. © 1998 Elsevier Science S.A. All rights reserved.

Keywords: Alkylidene; Cyclic voltammetry; Electrochemistry; Metalladithiolene; OTTLE; X-ray structure analysis

1. Introduction

The chemical and physical properties of alkylidene-bridged metalladithiolene complexes $[(Cp)M(S_2C_2Y_2)(CR^1R^2)]$ (M = Co and Rh) are presently under intensive investigations [1–3]. The three-membered ring is weakened by external stimulations like photoirradiation or chemical reagents to cause the opening of the ring. Although the redox chemistry of these complexes has received scant attention, Connelly et al. [4] have made the interesting observation that the oxidation of a μ-CH$_2$ complex of ruthenium $[Cp_2Ru_2(\mu\text{-CO})(\mu\text{-}$ dppm)$(\mu\text{-CH}_2)]$ results in the rapid loss of a proton from the CH$_2$ group to give a μ-alkylidyne-bridged complex; this can be easily functionalized by nucleophiles.

Furthermore, Geiger et al. [5] have reported that redox of μ-CR$_2$ complexes of dimetallic $[Cp_2M_2(CO)_n(\mu\text{-CR}_2)]$ ($n = 3$ or 4, M = Mn, Co, Rh) weakens the bonds in the M–C–M triangle to form mononuclear complexes.

Here, we wish to report electrochemical behavior for both the reduction and oxidation in a series of alkylidene-bridged metalladithiolene complexes $[(Cp)M(S_2C_2Y_2)(CR^1R^2)]$ (M = Co and Rh) from the viewpoint of effects of substituents and metal. The compounds studied are as shown, and the shorthand notations used to describe them in the text are as listed.

---

* Corresponding author. Tel.: + 81 3 32383446; fax: + 81 3 32383361; e-mail: c-takaya@hoffman.cc.sophia.ac.jp
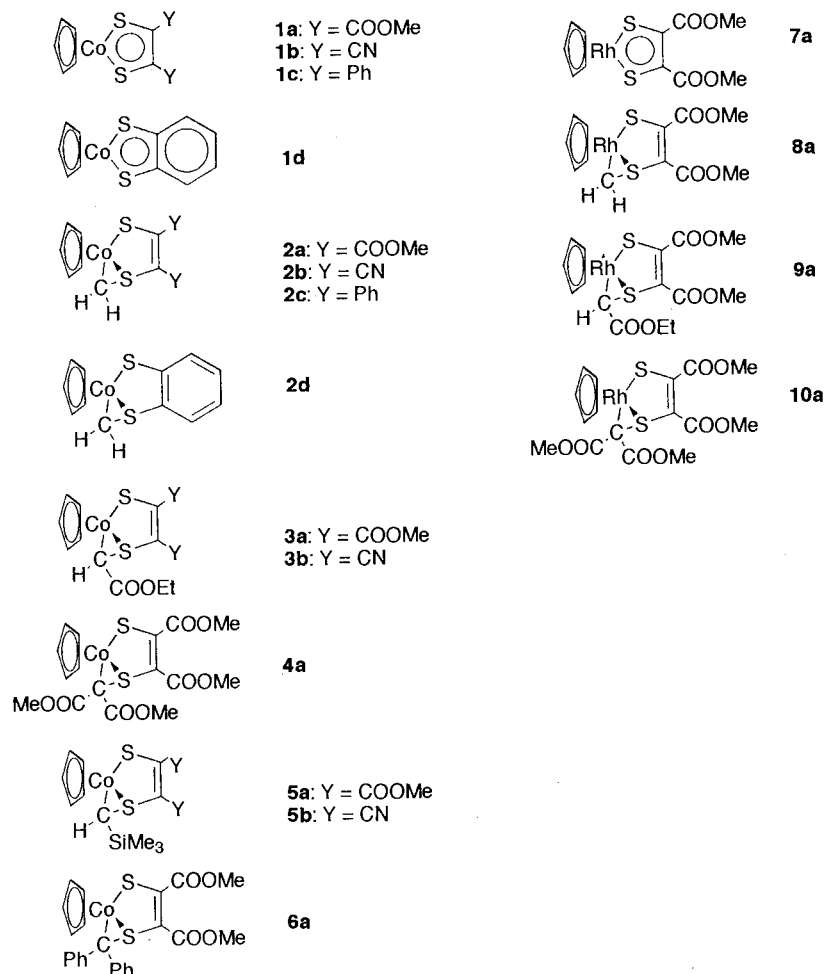
2. Experimental section

Reactions were carried out under argon by means of standard Schlenk techniques. NMR spectra were obtained on a JEOL GX-270 spectrometer. Mass and UV–vis spectra were obtained on a JEOL JMS-D300 spectrometer and Hitachi Model 228 UV–vis spectrometer, respectively. IR spectra were recorded on a Hitachi Model JMS-SX102A instrument. Anal found values were determined by using a Simazu PE2400-II instrument.

The dithiolene complexes $[(Cp)Co(S_2C_2Y_2)]$ (Y = COOMe (**1a**) [6], CN (**1b**) [7], Ph (**1c**) [8], $[(Cp)Co(S_2C_6H_4)]$ (**1d**) [9], and $[(Cp)Rh(S_2C_2(COOMe)_2)]$ (**7a**) [10] and the alkylidene-bridged complexes $[(Cp)M(S_2C_2Y_2)(CR^1R^2)]$ (**2a**, **2b**, **2c**, **2d**, **3a**, **5a**, **6a**, **8a**, **9a**, and **10a**) [11] were prepared by the literature methods.

2.1. Preparation of 3b and 5b

A solution of dithiolene complex **1b** (ca. 0.3 mmol) and diazo compound $N_2CR^1R^2$ $((R^1, R^2) = (H, COOEt)$ or $(H, SiMe_3))$ (ca. 1 mmol) in benzene (30

cm^3) was refluxed for 3 h. After the solvent was removed under reduced pressure, the residue was chromatographed on silica-gel (Wako-gel C-300, eluent: dichloromethane) and then the product was further submitted to HPLC (LC-08 produced by Japan Anal. Ind., column: JAIGEL-H, eluent: CHCl$_3$). An alkylidene-bridged complex **3b** or **5b** was obtained as a crystalline solid in 68 or 79% yield.

2.1.1. Identification of 3b

Dark brown crystal; M.p.: 167–168°C (decomp. to complex **1b**); ^{1}H-NMR (CDCl$_3$): δ 1.35 (t, ^3J(H–H) = 7.33 Hz, 3H, CH$_3$), 2.10 (s, 1H, CH carbene proton), 4.28 (q, ^3J(H–H) = 7.33 Hz, 2H, CH$_2$), and 5.28 (s, 5H, C$_5$H$_5$); ^{13}C-NMR (CDCl$_3$): δ 14.57 (CH$_2$CH$_3$; ^1J(C–H) 127 Hz), 32.65 (CHCOOC$_2$H$_5$; ^1J(C–H) = 177 Hz), 62.12 (CH$_2$CH$_3$; ^1J(C–H) = 148 Hz), 86.20 (Cp), 100.97 (dithiolene ring), 112.54 (CN), 114.14 (CN), 154.19 (COOC$_2$H$_5$), 176.80 (dithiolene ring); Mass spectrum (70 eV): m/z (relative intensity) 350 (87.4, M$^+$), 277 (76.11, M$^+$-COOEt), 264 (60.8, Cp-CoS$_2$C2(CN)$_2^+$), 251 (62.2, CpCoS$_2$C$_2$(CN)CH$^+$), 188 (100, CpCoS$_2^+$), 156 (38.6, CpCoS$^+$), 124 (98.7,

CpCo$^+$), and 59 (23.1, Co$^+$); IR(KBr disk) 2191, 1699, 1453, 1294, and 1153 cm^{-1}; UV–vis spectrum (CH$_2$Cl$_2$): λ 229.5 (ε 15045), 268.0 (16983), 435.5 (3007), and 540.5 (2059) nm; Found: C, 44.24; H, 3.13; N, 7.58%. Calcd for C$_{13}$H$_{11}$CoS$_2$N$_2$O$_2$: C, 44.58; H, 3.17; N, 8.00%.

2.1.2. Identification of 5b

Dark brown crystal; M.p. 194–196°C (decomp. to complex 1b); ^{1}H-NMR (CDCl$_3$): δ 0.26 (s, 9H, SiMe$_3$), 1.29 (s, 1H, CH), and 5.23 (s, 5H, C$_5$H$_5$); ^{13}C-NMR (CDCl$_3$) δ $-$0.18 (SiMe$_3$), 28.53 (^1J(C–H) = 143.45Hz, CHSiMe$_3$), 83.90 (Cp), 104.09 (dithiolene ring), 114.56 (CN), 115.21 (CN), and 151.75 (dithiolene ring); Mass spectrum (70 eV): m/z (relative intensity) 350 (44.4, M$^+$), 264 (7.3, CpCoS$_2$C$_2$(CN)$_2^+$), 251 (19.0, Cp-CoS$_2$C$_2$(CN)CH$^+$), 188 (9.2, CpCoS$_2^+$), 16 8 (5.2, Cp-CoSC$^+$), 156 (4.2, CpCoS$^+$), 124 (29.8, CpCo$^+$), 73 (100.0, SiMe$_3^+$), and 59 (11.9, Co$^+$); IR (KBr disk) 3110, 2952, 2185, and 1456 cm^{-1}; UV–vis spectrum (CH$_2$Cl$_2$): λ 264.4 (ε 18938), 316.8 (8239), and 535.2 (2516) nm; Found: C, 44.19; H, 4.27; N, 8.20; S, 18.21%. Calcd for C$_{13}$H$_{15}$CoS$_2$N$_2$Si: C, 44.56; H, 4.31; N, 7.99; S, 18.30%.

2.2. X-ray diffraction study

All measurements were made on a Rigaku AFC5S diffractometer with graphite-monochromated Mo–K$_\alpha$ radiation. The structure was solved by direct methods and expanded using Fourier techniques [12]. The non-hydrogen atoms were refined anisotropically. Idealized positions were used for the teXsan crystallographic software package of Molecular Structure Corporation [13]. Tables of atomic co-ordinates for non-hydrogen atoms, complete lists of bond lengths and angles, anisotropic displacement parameters, and hydrogen co-ordinates and isotropic displacement parameters are available as supporting information.

2.3. Crystal structure data for 1a

A dark-purple prismatic crystal of C$_{11}$H$_{11}$CoO$_4$S$_2$ (FW = 330.26), monoclinic, space group $P2_1/c$ (#14), $a = 6.254(3)$ Å, $b = 21.827(4)$ Å, $c = 9.890(3)$ Å, $\beta = 101.75(4)°$, $V = 1321.7(8)$ Å^3, $Z = 4$, $D_{calc} = 1.660$ g cm^{-3}, μ(Mo–K$_\alpha$) = 16.16 cm^{-1}, $F(000) = 672.00$, $R = 0.045$ ($Rw = 0.031$) on 1713 intensities ($|F_o| > 3.00\sigma|F_o|$).

2.4. Crystal structure data for 1b

A dark-purple prismatic crystal of C$_9$H$_5$CoN$_2$S$_2$ (FW = 264.21), monoclinic, space group $C2/c$ (#15), $a = 17.070(2)$ Å, $b = 8.485(2)$ Å, $c = 14.821(2)$ Å, $\beta = 109.485(9)°$, $V = 2023.7(5)$ Å^3, $Z = 8$, $D_{calc} = 1.734$ g cm^{-3}, μ(Mo–K$_\alpha$) = 20.64 cm^{-1}, $F(000) = 1056.00$,

$R = 0.043$ ($Rw = 0.039$) on 1535 intensities ($|F_o| > 3.00\sigma|F_o|$).

2.5. Crystal structure data for 1c

A dark-blue cubic crystal of C$_{19}$H$_{15}$CoS$_2$ (FW = 366.38), monoclinic, space group $P2_1/n$ (#14), $a = 16.065(3)$ Å, $b = 6.116(6)$ Å, $c = 16.478(4)$ Å, $\beta = 91.90(2)°$, $V = 1618(1)$ Å^3, $Z = 4$, $D_{calc} = 1.504$ g cm^{-3}, μ(Mo–K$_\alpha$) = 13.11 cm^{-1}, $F(000) = 752.00$, $R = 0.089$ ($Rw = 0.080$) on 1601 intensities ($|F_o| > 3.00\sigma|F_o|$).
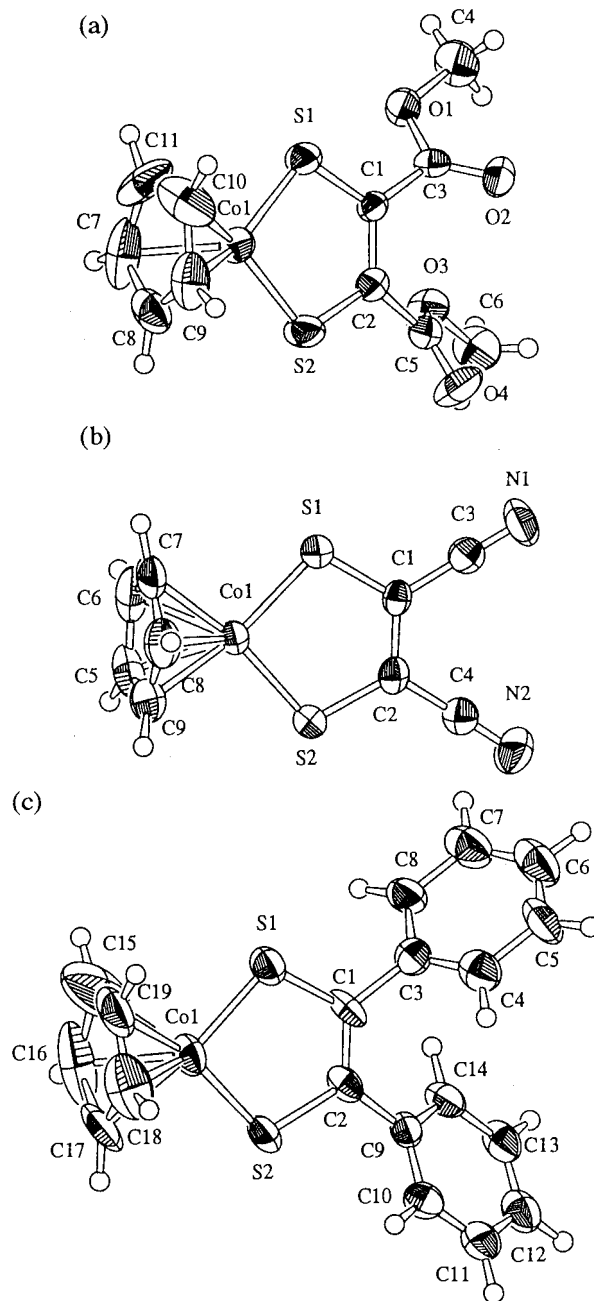

Fig. 1. X-ray crystal structure of original metaladithiolene complexes: (a) 1a, (b) 1b, and (c) 1c.

Table 1
Selected bond lengths (Å) of original dithiolene complexes

	1a	1b	1c
Co–S(1)	2.108(2)	2.110(2)	2.110(4)
Co–S(2)	2.104(1)	2,109(2)	2.098(4)
S(1)–C(1)	1.716(4)	1.706(6)	1.75(1)
S(2)–C(2)	1.718(4)	1.710(5)	1.73(1)
C(1)–C(2)	1.368(5)	1.710(5)	1.35(2)
Cp–Co	1.652	1.645	1.6392

2.6. Crystal structure data for 2a

A dark-brown prismatic crystal of $C_{12}H_{13}CoO_4S_2$ (FW = 344.29), triclinic, space group $P\bar{1}$ (# 2), $a = 10.466(1)$ Å, $b = 14.028(3)$ Å, $c = 10.382(1)$ Å, $\alpha = 107.17(1)°$, $\beta = 104.93(1)°$, $\gamma = 93.13(1)°$, $V = 1393.1(4)$ Å^3, $Z = 4$, $D_{calc} = 1.641$ g cm^{-3}, $\mu(Mo-K_\alpha) = 15.36$ cm^{-1}, $F(000) = 704.00$, $R = 0.036$ ($Rw = 0.023$) on 3224 intensities ($|F_o| > 3.00\sigma|F_o|$).

2.7. Crystal structure data for 2d

A dark-purple prismatic crystal of $C_{12}H_{11}CoS_2$ (FW = 278.27), monoclinic, space group $P2_1/c$ (# 14), $a = 9.088(2)$ Å, $b = 7.554(2)$ Å, $c = 16.340(1)$ Å, $\beta = 96.17(1)°$, $V = 1115.3(3)$ Å^3, $Z = 4$, $D_{calc} = 1.657$ g cm^{-3}, $\mu(Mo-K_\alpha) = 18.72$ cm^{-1}, $F(000) = 568.00$, $R = 0.026$ ($Rw = 0.028$) on 1961 intensities ($|F_o| > 3.00\sigma|F_o|$).

2.8. Crystal structure data for 3a

A dark-brown prismatic crystal of $C_{15}H_{17}CoO_6S_2$ (FW = 416.35), monoclinic, space group $C2/c$ (# 15), $a = 20.26(1)$ Å, $b = 9.572(9)$ Å, $c = 17.96(1)$ Å, $\beta = 93.45(5)°$, $V = 3476(3)$ Å^3, $Z = 8$, $D_{calc} = 1.591$ g cm^{-3}, $\mu(Mo-K_\alpha) = 12.55$ cm^{-1}, $F(000) = 1712.00$, $R = 0.056$ ($Rw = 0.052$) on 1556 intensities ($|F_o| > 3.00\sigma|F_o|$).

2.9. Crystal structure data for 5a

A dark-brown prismatic crystal of $C_{19}H_{21}CoO_4S_2Si$ (FW = 416.47), monoclinic, space group $P2_1/a$ (# 14), $a = 11.727(2)$ Å, $b = 11.640(2)$ Å, $c = 14.997(2)$ Å, $\beta =$

$112.502(10)°$, $V = 1891.2(5)$ Å^3, $Z = 4$, $D_{calc} = 1.463$ g cm^{-3}, $\mu(Mo-K_\alpha) = 12.06$ cm^{-1}, $F(000) = 864.00$, $R = 0.038$ ($Rw = 0.028$) on 2778 intensities ($|F_o| > 3.00\sigma|F_o|$).

2.10. Crystal structure data for 6a

A dark-purple prismatic crystal of $C_{24}H_{21}CoO_4S_2$ (FW = 496.48), monoclinic, space group $C2/c$ (# 15), $a = 27.36(1)$ Å, $b = 7.755(3)$ Å, $c = 24.37(1)$ Å, $\beta = 119.72(2)°$, $V = 4489(2)$ Å^3, $Z = 8$, $D_{calc} = 1.469$ g cm^{-3}, $\mu(Mo-K_\alpha) = 9.79$ cm^{-1}, $F(000) = 2048.00$, $R = 0.063$ ($Rw = 0.058$) on 2948 intensities ($|F_o| > 3.00\sigma|F_o|$).

2.11. Crystal structure data for 10a

A dark-red cubic crystal of $C_{16}H_{17}O_8RhS_2$ (FW = 504.33, triclinic, space group $P1$ (# 2), $a = 8.0661(2)$ Å, $b = 15.782(4)$ Å, $c = 7.787(3)$ Å, $\alpha = 95.34(3)°$, $\beta = 102.88(3)°$, $\gamma = 97.44(3)°$, $V = 950.0(6)$ Å^3, $Z = 2$, $D_{calc} = 1.763$ g cm^{-3}, $\mu(Mo-K_\alpha) = 11.58$ cm^{-1}, $F(000) = 508.00$, $R = 0.024$ ($Rw = 0.021$) on 3786 intensities ($|F_o| > 3.00\sigma|F_o|$).

2.12. Measurements

The voltammetric equipment and the optically transparent thin-layer electrochemical electrode (OTTLE) cell used here were described previously [14,15].

The electrochemical measurements were undertaken in acetonitrile solutions containing 0.1 mol dm^{-3} tetraethylammonium perchlorate (TEAP) at 25°C, unless there were special circumstances.

A stationary platinum disk (1.6 mm in diameter) (CV), platinum gauze (controlled potential coulometry), or platinum mesh (OTTLE) was used as a working electrode. A platinum wire served as a counter electrode, with the reference electrode as Ag|Ag$^+$ corrected for junction potentials by being referenced internally to the ferrocene/ferrocenium (Fc|Fc$^+$) couple.

ESR spectra were obtained for ca. 1 mmol dm^{-3} solutions of ethanol and toluene 1:1 mixture of the complex with excess NaBH$_4$ at 77 K. The instruments used here have been described previously [14].

3. Results and discussion

3.1. Structure of alkylidene-bridged complexes

The molecular structures of complexes **1a**, **1b**, and **1c** have been determined by X-ray crystal structure analysis (Fig. 1). The five-membered metalladithiolene rings are almost planar in these complexes. The selected bond lengths and angles of these complexes are shown in Tables 1 and 2.
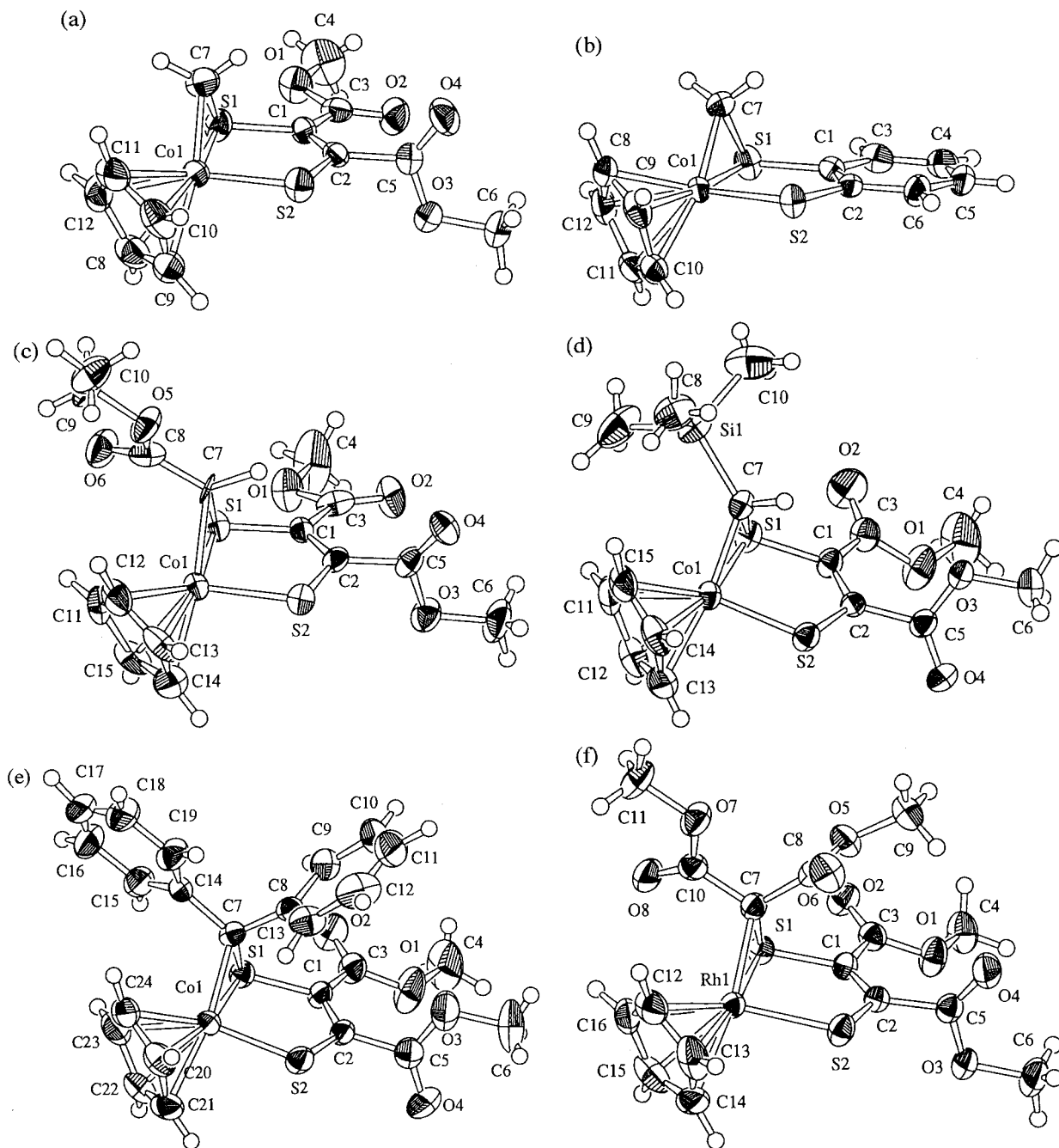
Table 2
Selected bond angles (°) of original dithiolene complexes

	1a	1b	1c
S(1)–Co–S(2)	92.2(5)	93.05(7)	91.0(2)
Co–S(1)–C(1)	105.0(2)	104.6(2)	105.5(4)
Co–S(2)–C(2)	104.7(2)	104.2(2)	106.7(5)
S(1)–C(1)–C(2)	118.7(4)	118.8(4)	118.6(9)
S(2)–C(2)–C(1)	119.4(4)	119.3(5)	118(1)

Fig. 2. X-ray crystal structure of alkylidene-bridged metaladithiolene complexes: (a) **2a**, (b) **2d**, (c) **3a**, (d) **5a**, (e) **6a**, (f) **10a**.

The molecular structures of alkylidene-bridged complexes **2a**, **2d**, **3a**, **5a**, **6a**, and **10a** were also determined by X-ray crystal structure analysis (Fig. 2). The selected bond lengths and angles of these complexes are shown in Tables 3 and 4. The almost planar five-membered metalladithiolene rings are retained and the three-membered ring of alkylidene moieties are almost perpendicular to the dithiolene rings in these complexes. The metal-S and metal-C bond distances in the rhodium complexes are longer than those of cobalt complexes. Further, the

C–C bond lengths of the dithiolene ring in the bridging complexes are slightly shorter than the corresponding values in the original dithiolene complexes. Such results suggest that the contribution of the dithioolefinic structure becomes important and aromatic properties of dithiolene ring become small, due to the formation of a bridging structure (Scheme 1). On the other hand, M–S bond lengths become long, resulting from the formation of a bridging structure. It shows the relaxation of unsaturation properties in the dithiolene ring.

Table 3
Selected bond lengths (Å) of alkylidene-bridged complexes

	2a	2d	3a	4a [16]	5a	6a	10a
M–S(1)	2.184(1)	2.1828(6)	2.189(3)	2.182(1)	2.1855(9)	2.166(2)	2.3008(6)
M–S(2)	2.207(1)	2.2281(6)	2.219(2)	2.216(1)	2.2189(9)	2.209(2)	2.3223(7)
S(1)–C(1)	1.769(4)	1.773(2)	1.788(10)	1.765(2)	1.768(3)	1.763(5)	1.769(2)
S(2)–C(2)	1.692(4)	1.741(2)	1.715(10)	1.703(2)	1.703(3)	1.693(6)	1.705(2)
C(1)–C(2)	1.366(5)	1.405(3)	1.36(1)	1.361(3)	1.370(4)	1.361(7)	1.359(3)
M–C(7)	1.942(4)	1.944(2)	2.028(10)	2.001(2)	1.983(3)	2.008(6)	2.112(2)
S(1)–C(7)	1.749(5)	1.762(3)	1.807(9)	1.749(3)	1.778(3)	1.798(6)	1.792(2)
Cp–M	1.688	1.691	1.682	1.681	1.691	1.693	1.830

Table 4
Selected bond angles (°) of alkylidene-bridged complexes

	2a	2d	3a	4a [16]	5a	6a	10a
S(1)–M–S(2)	91.75(4)	91.59(2)	91.7(1)	91.77(3)	90.99(3)	91.95(6)	88.03(2)
M–S(1)–C(1)	103.4(1)	104.78(7)	103.4(3)	103.29(8)	104.1(1)	103.6(2)	103.94(7)
M–S(2)–C(2)	102.3(1)	103.47(7)	102.3(3)	102.40(8)	103.1(1)	102.2(2)	103.18(7)
S(1)–C(1)–C(2)	117.6(3)	118.7(2)	117.8(7)	118.9(2)	118.0(2)	118.2(4)	119.7(2)
S(2)–C(2)–C(1)	124.6(3)	121.4(2)	124.2(7)	123.5(2)	123.3(2)	124.1(4)	124.8(2)
S(1)–M–C(7)	49.7(1)	50.15(8)	50.6(3)	50.56(7)	50.21(8)	50.8(2)	47.69(6)
S(2)–M–C(7)	94.2(2)	93.48(8)	91.32(3)	96.28(8)	93.45(9)	97.6(2)	92.18(6)
M–S(1)–C(7)	57.9(2)	57.89(8)	60.1(3)	59.50(8)	59.0(1)	60.0(2)	60.63(7)
C(1)–S(1)–C(7)	105.2(2)	103.0(1)	101.8(5)	105.2(1)	105.2(1)	105.3(3)	105.2(1)
M–C(7)–S(1)	72.4(2)	71.96(9)	69.3(4)	69.94(9)	70.8(1)	69.1(2)	71.68(8)

3.2. Electrochemistry of alkylidene-bridged complexes

3.2.1. Electrochemistry of [CpCo(S₂C₂(COOMe)₂(CH₂)] (2a)

At first, we describe the electrochemical behavior of [CpCo(S$_2$C$_2$(COOMe)$_2$(CH$_2$)] (2a) using CV and OTTLE. This OTTLE cell was used for in situ measurement of the visible absorption spectra during electrolysis. The thickness of thin layer in this OTTLE cell is 0.4 mm. A platinum gauze was used as a working electrode. The spectro-multichannel photodetector for spectral measurement of OTTLE permits spectral measurement per 0.1 s. The use of this OTTLE cell makes possible to measure CV at very slow rate ($= 1$ mV s^{-1}) and to determine approximately the yields of products, because the thin-layer cell can prevent the diffusion of solution. So, this OTTLE system is very useful for products analysis of electrochemistry.

Fig. 3 displays CV scan of 2a (solid line) together with that of the corresponding original complex 1a (dashed line).
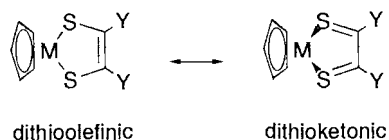
Scheme 1. Aromatic properties.

3.2.1.1. Reduction.
Complex 2a displays reversible reduction in CV results (Fig. 3a). The value of the half wave potential ($E_{1/2}$) of reduction of 2a (-1.60 V vs. Fc|Fc$^+$) is more negative than that of 1a (-0.94 V). The electrochemical reduction of 2a displays no scan rate dependence in the range of 20–200 mVs^{-1}, and it exhibits current ratios (i_{pa}/i_{pc}) $=$ ca. 1, indicative of a chemically reversible process.

An in situ measurement of the electronic absorption spectra during the electrolytic reduction using an optically transparent thin-layer electrode (OTTLE) showed the reversibility of the reduction and re-oxidation. Fig. 4a shows the spectral changes during the controlled potential electrolysis (at -1.70 V) using OTTLE. The absorption around 500 nm decreased as the reduction proceeds. Then in the spectra obtained after the re-oxidation (Fig. 4b), the absorption around 500 nm increased and completely agreed with the original spectra. Namely, 2a showed reversible reduction behavior on these time scales.

Next, controlled potential coulometry was applied. Bulk electrolysis of 2a at -1.70 V (more negative than its reduction potential) which requires about 1 Faraday ($n = 1$) for 30 min, caused the color change from brown to light yellow. After evaporation of the solvent under air atmosphere and the extraction with dichloromethane, the products were chromatographed on an alumina column with dichloromethane as eluent. The resulting purple material displayed ^{1}H-NMR spectra which are consistent with those of the original complex 1a (yield 14%, recovery 48%).
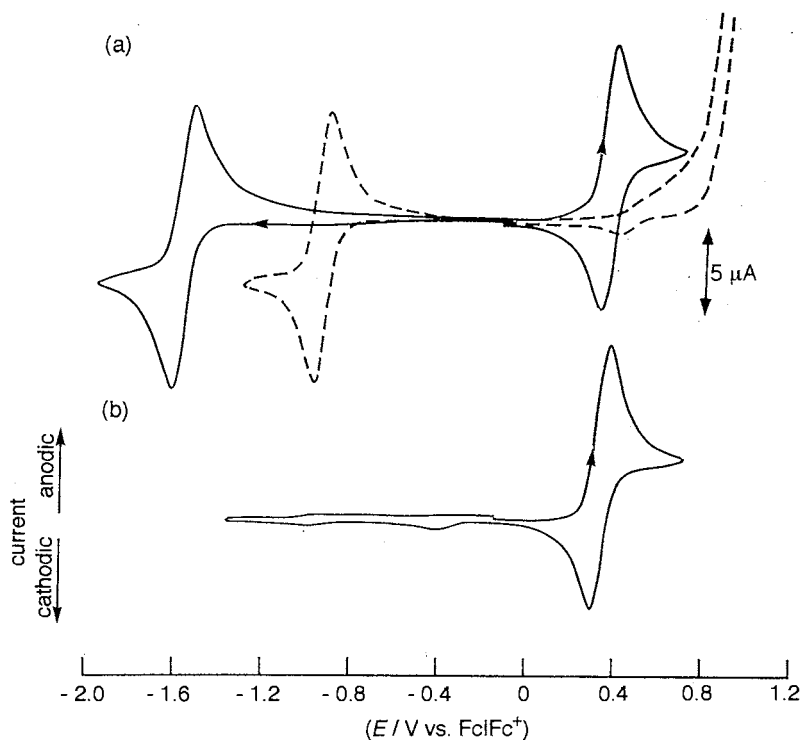
Fig. 3. Cyclic voltammogram ($v = 100$ mV s^{-1}, $\Phi = 1.6$ mm Pt disk) of 1 mM complex in CH$_3$CN containing 0.1 M TEAP: (a) **2a** (—) and **1a** (- - -), (b) **2a**, initial slope is to positive.

Furthermore, we attempted to observe the ESR spectra of **2a**$^-$, but **2a**$^-$ is unstable to detection by ESR spectroscopy, and we observed instead the ESR spectra of **1a**$^-$ [16].

Because the anion **1a**$^-$ is re-oxidized by the air, these data strongly suggest that the radical anion **2a**$^-$ formed in the initial reduction process eliminates the methylene moiety slowly to give **1a**$^-$ (Scheme 2).

Namely, the methylene-bridged anion radical is too unstable to be isolated in pure form. One electron reduction of **2a** affords an anion radical having a few minutes of lifetime and then it eliminates the alkylidene moiety to give more stable **1a**$^-$.

3.2.1.2. Oxidation.
In the oxidation, CV of complex **2a** showed reversible peaks at 0.34 V, which is more negative than that of the corresponding original complex **1a** (0.88 V). The formation of the adduct makes the oxidation state of the complex more stable.

But if the potential scan is continued to the more negative range after its re-reduction, two more small cathodic peaks appear at -0.4 and -1.0 V (Fig. 3b). The latter corresponds to the reduction of the original complex **1a**. These suggest that the lifetime of cation radical **2a**$^+$ is not so long. Therefore, an OTTLE measurement was attempted. Fig. 5a shows the spectral change during the controlled potential electrolysis during the first 6 s (at 0.5 V). The absorption around 500 nm decreased as the oxidation proceeds. During only the first 6 s, isosbestic points were observed, but further reaction

(>6 s) brings about another type of spectral change (Fig. 5c). And the spectra obtained after the re-oxidation within 6 s agrees with the original spectra of **2a** (Fig. 5b). However, prolonged oxidation (>6 s) causes an irreversible reaction: Even if we return the potential to the initial value (0 V), no spectral change are observed. If we set the potential at -0.5 V (more negative range than the first small peaks) after 210 s, a new absorption appears around 550 nm, which is ascribed to the original complex **1a** (yield 17% in this time scale) (Fig. 5d).

Namely, the cation radical **2a**$^+$ has a few seconds of lifetime, and then it is converted to a species X$^+$, of which the re-reduction potential value is -0.4 V. When the species X$^+$ was re-reduced, **1a** was rapidly generated. The complex X$^+$ is stable, but the neutral X is very unstable (Scheme 3).
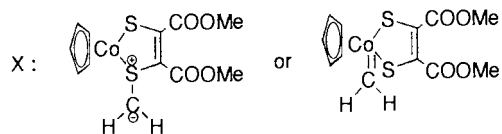
The structure of the complex X formed by the oxidation has not yet been clarified, but it would be a product in which the Co–C or S–C bond is cleaved, because X easily gives the original complex **1a**. We could succeed in detecting the intermediary species in the elimination process. This is one of the very rare and important successes in the trapping of the intermediate in the elimination mechanism.
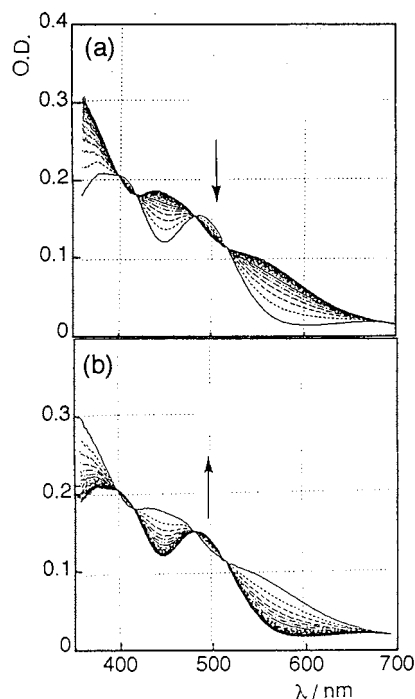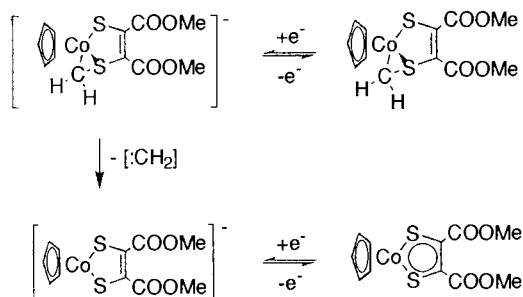
Fig. 4. Electronic spectral change of **2a** during (a) reduction and (b) re-oxidation: sampling interval, 1 s; potential stepped from (a) − 0.5 to − 1.7 V and (b) − 1.7 to − 0.5 V vs. Fc|Fc⁺ using OTTLE system.

3.2.2. Effect of substituents in the bridging groups; [Cp-Co(S₂C₂(COOMe)₂ (CR¹R²)] (2a, 3a, 4a, 5a, 6a) and [CpCo(S₂C₂(CN)₂(CR¹R²)](2b, 3b, 5b) and in the dithiolene ring [CpCo(S₂C₂Y₂(CH₂)] (2a, 2b, 2c, 2d)

Fig. 6 displays CV scans of **3a**, **5a**, and **6a**. Table 5 lists the value of half wave potentials for all redox reactions described in this paper. Unlike **4a**, the alkylidene-bridged complexes **3a**, **5a**, and **6a** exhibit well-defined reversible or quasi-reversible one-electron reduction waves. The reversible one-electron reduction waves of the original complexes are ascribed to the reduction of the central metal atom [17]. Like the original complexes, the alkylidene-bridged complexes are expected to undergo electron transfer to the central metal. Complexes **5a** and **6a** showed a quasi-reversible reduction wave; if one continued the potential scan to a more positive range than its re-oxidation, one more small anodic peaks appeared at − 1.0 V. These oxidation peaks are ascribed to the re-oxidation of **1a⁻**.

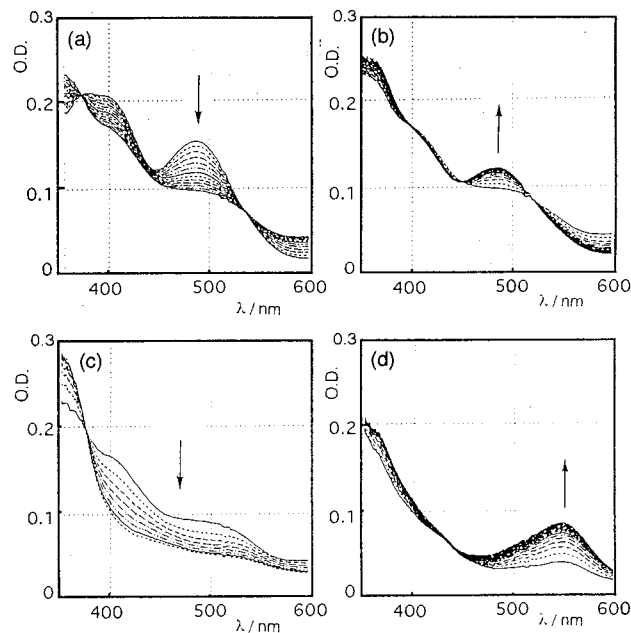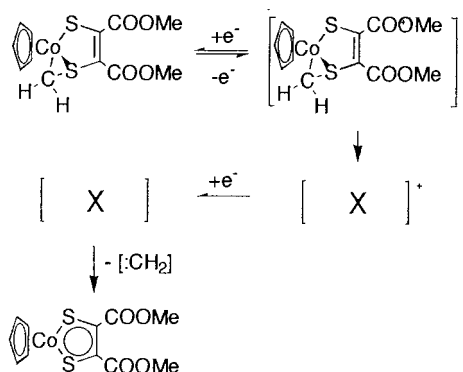Scheme 2. Reaction mechanism of reduction process.

Fig. 5. Electronic spectral change of **2a** during oxidation and re-reduction: (a) potential stepped from − 0.1 to 0.5 V; sampling interval, 0.5 s; sampling time, 0–6 s, and (b) potential stepped from 0.5 to − 0.1 V; sampling interval, 0.5 s; sampling time, 6–16 s, (c) potential stepped from − 0.1 to 0.5 V; sampling interval, 4 s sampling time, 6–34 s, and (d) potential stepped from − 0.1 to − 0.5 V; sampling interval, 10 s; sampling time, 210–410 s, vs. Fc|Fc⁺.

The formation of **1a⁻** is also supported by the electrochemical investigation using controlled potential coulometry and ESR. The product by the electrochemical reaction was **1a**. In the ESR investigations of these anion radical, we also observed the ESR spectra of **1a⁻**.

Namely, these reduction products **3a⁻**, **5a⁻**, and **6a⁻** have lifetimes of a few minutes. These are shorter than that for **2a⁻**. They are transformed to **1a⁻**, accompanied by the elimination of the alkylidene moiety.

Other alkylidene-bridged cobalt complexes **2b**, **3b**, **5b**, **2c**, and **2d** also exhibit the same behavior as **2a**. They showed reversible reduction wave at a more negative potential than original complexes. And they changed to anion radicals of original complexes after a few minutes.

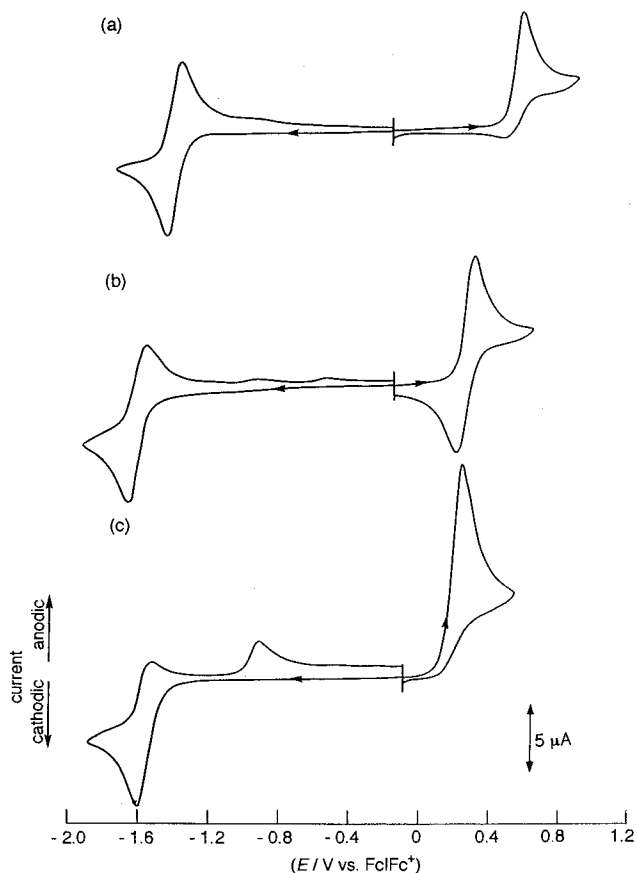Scheme 3. Reaction mechanism of oxidation process.

Fig. 6. Cyclic voltammogram ($v = 100$ mV s^{-1}, $\Phi = 1.6$ mm Pt disk) of 1 mM complex in CH$_3$CN containing 0.1 M TEAP: (a) **3a**, (b) **5a**, and (c) **6a**.

Each of the oxidation peaks of **2c** and **5a** is accompanied by a corresponding re-reduction peak due to the reversibility of its oxidation process at 25°C. The CV of other complexes showed a single oxidation peak corresponding to a Nernstian one-electron process, but the oxidized form is unstable and rapidly dissociates into the neutral original complex **1**, followed by further chemical reactions similarly to **2a**. Interestingly, at −40°C, the oxidized forms of **3a**, **2b**, and **2d** are stable and each of them shows a pair of peaks, due to the reversibility of their oxidation process (Fig. 7).

The half-wave potentials ($E_{1/2}$) of reduction reflect the electron densities of the central metal and those of oxidation reflect those of the sulfur atoms. Redox potentials of the complexes display a marked dependence on the nature of the substituents in the bridging alkylidene moieties. The more electron-withdrawing are the substituents, the lower are the half-wave potentials of the complexes. These results suggest that the increases in the electron density at the dithiolene ring are due to the bridging of alkylidene between Co and S.

3.2.3. Effect of the metals; [CpRh(S$_2$C$_2$(COOMe)$_2$(CR^{1}R^2)] (8a, 9a, 10a)

Typical cyclic voltammograms of the rhodium alkyli-

dene-bridged complexes together with that of the original complex, are shown in Fig. 8.

3.2.3.1. Original rhodiadithiolene complexes (7a).
The original rhodium complex **7a** exhibits a well-defined reversible one-electron reduction wave similarly to the case of the cobalt complex [17]. The reduction potential of complex **7a** is more negative than that of the corresponding cobalt complex **1a**. The reduction potential is a measure of the electron density at the metal atom. In the reactions of dithiolene complexes with diazo compounds, the alkylidene-bridged rhodium complexes were obtained in higher yields than the cobalt complexes. Those reactions are initiated by nucleophilic attack of the diazo compounds to the metal. This discrepancy may be explained by the softness of rhodium.

3.2.3.2. Alkylidene-bridged rhodium complexes.
All alkylidene-bridged complexes exhibit irreversible reduction waves measured by the scan rate of 100 mV s^{-1}. However, complex **9a** showed a quasi-reversible wave under rapid scan ($v > 200$ mV s^{-1}). The lifetimes of the rhodium anions are shorter than those of the corresponding cobalt anions. In the reduction of the complexes **10a**, a re-oxidation wave was also exhibited at a more positive potential, which implies the presence of another reduction product which exhibits a re-oxidation wave due to the chemical reaction after the charge transfer. This behavior is the same as that of **4a** and the reduction leads to the formation of the ylide structure due to the bond cleavage of the metal–carbon bond (Scheme 4).

The effects of substituents in the bridging groups are similar to those in the cobalt complexes. The redox potentials are linear with the number of the ester groups in the alkylidene moiety (Fig. 9). The reduction of alkylidene-bridged metalladithiolene complexes occurs at the metal site. The reduction potentials of Rh(III) complexes are about 0.3 V more negative than those of the corresponding Co(III) complexes, probably due to the higher electronegativity of rhodium.

The oxidation of the alkylidene-bridged rhodium complexes is irreversible. In contrast to reduction, the oxidation waves of the rhodium complexes appear at more positive potentials than those of the corresponding cobalt complexes. The gaps between reduction and oxidation potentials in rhodium complexes are larger than those of cobalt complexes. These results agreed with those of [CpMcod] [18] and [CpM(CO)$_2$] [19] (M = Co and Rh). The shift of half-wave potential $E_{1/2}$ from Co to Rh for oxidation is smaller than that for reduction. This small shift of oxidation potential would indicate that the oxidation occurs at the sulfur atoms which are less affected by metal atoms.

Table 5
Electrochemical data (vs. Fc|Fc$^+$).

	Reduction				Oxidation			
	$E^a_{1/2}$ (V)	ΔE^b (mV)	ΔE^c_p (mV)	I_{pa}/I^d_{pc}	$E^a_{1/2}$ (V)	Δe^b (mV)	Δe^c_p (mV)	I_{pc}/I^d_{pa}
1a	−0.94	62	56	1	0.88	88		
1b	−0.62	68	56	1	0.71	56	79	1
1c	−0.19	64	69	1	0.31	90	173	1
1d	−1.00	57	57	1	0.38	106		
7a	−1.20	65	65	1	0.50	56	72	1
2a	−1.60	66	88	1	0.34	60	56	1
3a	−1.37	76	130	1	0.57	56		
4a [16]	−1.25	86	487	1	0.66	57		
5a	−1.67	89	187	0.6	0.30	68	129	0.8
6a	−1.56	72	80	0.4	0.23	65		
2b	−1.22	71	112	1	0.60	62		
3b	−1.05	72	122	1	0.76	64		
5b	−1.14	66	88	1	0.52	67		
2c	−1.68	65	90	1	0.00	59	60	0.8
2d	−1.57	82	90	1	−0.06	68		
8a	−1.85	52			0.46	54		
9a	−1.70	57	50	0.1	0.69	50		
10a	−1.43	64	400	0.4	0.77	55		

^{a} $E_{1/2} = (E_p + E_{p/2})/2$, as half potential.
^{b} $\Delta E = E_p - E_{p/2}$.
^{c} $\Delta E_p = |E_{pa} - E_{pc}|$
^{d} I_{pa} = anodic peak current; I_{pc} = cathodic peak current

4. Conclusions

1. In the molecular structures of alkylidene-bridged complexes, the almost planar five-membered metalla-dithiolene rings are retained and the directions of alkylidene moieties are almost perpendicular to the dithiolene rings. The C–C bond lengths of the dithiolene ring in the bridging complexes are shorter than the corresponding value in the original dithiolene complexes. But M–S bond lengths become long as the formation of the bridging structure progresses;

2. One-electron reduced products of alkylidene-bridged complexes have a few minutes lifetime and then they lose the alkylidene-bridged moiety to give the stable anion radicals of the original dithiolene complexes;

3. The cations of alkylidene-bridged complexes have a few seconds lifetime, and then they change to some other species. When they were re-reduced, the corresponding original dithiolene complexes were formed rapidly. This structurally changed species was stable in the cationic form, but they were very unstable in the neutral form to decompose original complexes and alkylidene moiety;

4. In the alkylidene-bridged complexes, the trend is for more electron-withdrawing substituents to show more positive redox potentials;

5. Rhodium complexes have more negative reduction potentials, but more positive oxidation potentials, than cobalt complexes. The gaps between reduction and oxidation potentials in rhodium complexes are larger than those in cobalt complexes;

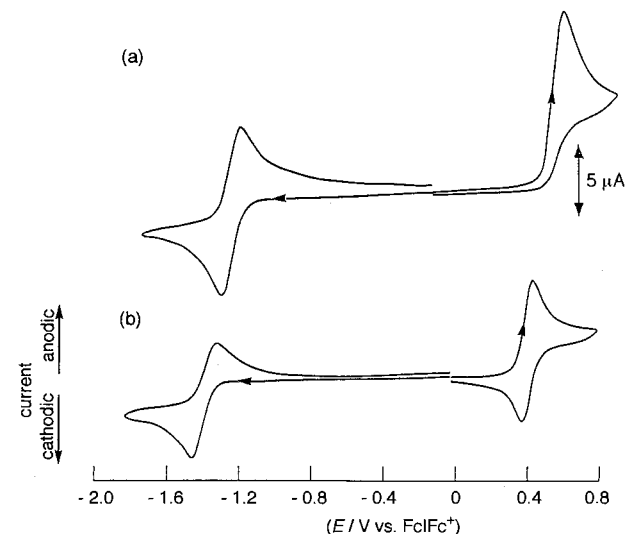6. The lifetime of anions of rhodium complexes are shorter than those of the cobalt complexes.

5. Supporting information available

Tables giving crystal data and refinement details, positional and thermal parameters and bond distances and angles (216 pages). Ordering information is given on any current masthead page.
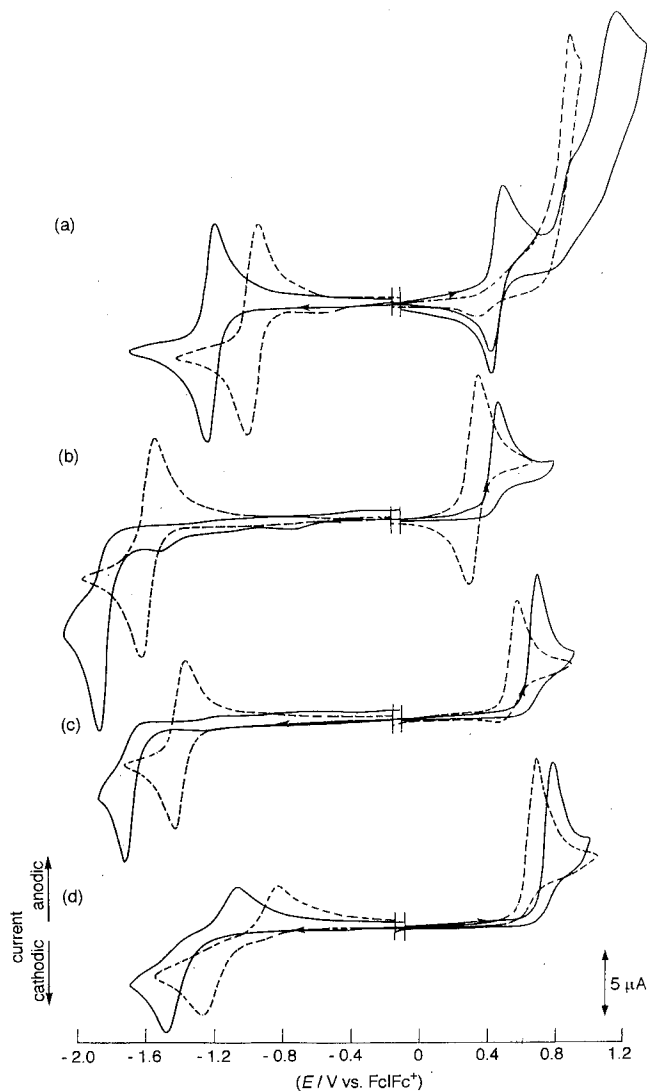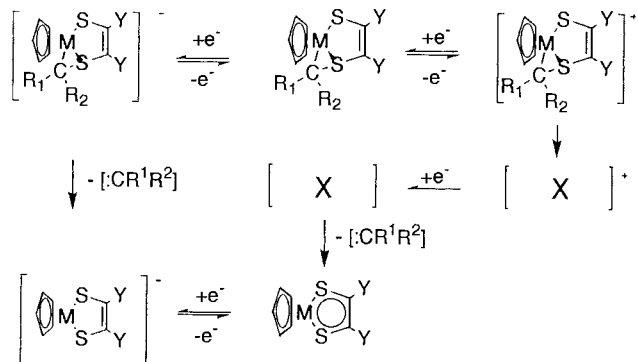

Fig. 7. Cyclic voltammogram ($v = 100$ mV s^{-1}, $\Phi = 1.6$ mm Pt disk) of 1 mM complex **2b** in CH$_3$CN containing 0.1 M TEAP at (a) 25°C and (b) −40°C.
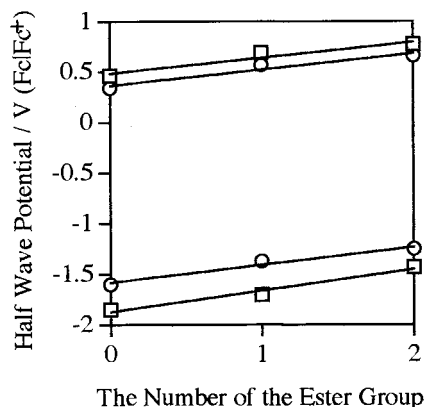
Fig. 9. The number of the ester groups in alkylidene moiety vs the value of half wave potential $E_{1/2}$ plot for cobalt (○) and rhodium (□) alkylidene-bridged dithiolene complexes.

References

[1] C. Takayama, N. Sakamoto, T. Harada, et al., Organometallics 15 (1996) 5077.

[2] M. Sakurada, M. Kajitani, H. Hatano, et al., Organometallics 11 (1992) 2337.

[3] M. Kajitani, F. Kawakita, E. Chikuma, M. Sakurada, T. Akiyama, A. Sugimori, Chem. Lett. (1995) 85.

[4] N.G. Connelly, N.J. Forrow, B.P. Gracey, S.A.R. Knox, A.G. Orpen, J. Chem. Soc., Chem. Commun. (1985) 14.

[5] W.E. Geiger, T. Gennett, W.K. McVicar, Organometallics 6 (1987) 1634.

[6] H. Boennemann, B. Bogdanovic, W. Brijoux et al., Transition-metal-catalyzed synthesis of heterocyclic compounds, in: J.R. Kosak (Ed.), Catalysis in Organic Reactions, Marcel Dekker, New York, 1984, pp. 31–62.

[7] J. Locke, J.A. McCleverty, Inorg. Chem. 5 (1966) 1157.

[8] M. Kajitani, R. Ochiai, K. Dohki, et al., Bull. Chem. Soc. Jpn. 62 (1986) 3266.

[9] R.B. King, C.A. Eggers, Inorg. Chem. 4 (1968) 424.

[10] M. Kajitani, T. Suetsugu, T. Takagi, J. Organomet. Chem. C8 (1995) 487.

[11] M. Sakurada, M. Kajitani, K. Dohki, T. Akiyama, A. Sugimori, J. Organomet. Chem. 423 (1992) 144.

[12] P.T. Beurskens, G. Admiraal, G. Beurskens, et al., The DIRDIF Program System. Technical Report of the Crystallography Laboratory, University of Nijmegen, Nijmegen, The Netherlands, 1992.

[13] teXsan: Crystal Structure Analysis Package; Molecular Structure Corporation: 1985, 1992.

[14] H. Ushijima, M. Kajitani, K. Shimizu, G.P. Sato, T. Akiyama, A. Sugimori, Appl. Organomet. Chem. 5 (1991) 221.

[15] K. Shimizu, H. Ikehara, M. Kajitani, H. Ushijima, T. Akiyama, A. Sugimori, G.P. Sato, J. Electroanal. Chem 396 (1995) 465.

[16] C. Takayama, M. Kajitani, T. Sugiyama, T. Akiyama, K. Shimizu, A. Sugimori, Organometallics 16 (1997) 3498.

[17] H. Ushijima, M. Kajitani, K. Shimizu, G.P. Sato, T. Akiyama, A. Sugimori, J. Electroanal. Chem. 303 (1991) 199.

[18] N.G. Connelly, W.E. Geiger, G.A. Lane, S.J. Raven, P.H. Rieger, J. Am. Chem. Soc. 108 (1986) 6219.

[19] D.L. Lichtenberger, D.C. Calabro, G.E. Kellogg, Organometallics 3 (1984) 1623.

Fig. 8. Cyclic voltammogram ($v = 100$ mV s^{-1}, $\Phi = 1.6$ mm Pt disk) of 1 mM complex in CH$_3$CN containing 0.1 M TEAP: (a) **7a** (—) and **1a** (- - -), (b) **8a** (—) and **2a** (- - -), (c) **9a** (—) and **3a** (- - -), and (d) **10a** (—) and **4a** (- - -).

Acknowledgements

Scheme 4. Electrochemical behavior of alkylidne-bridged metalladithiolene complexes.